Experimental studies on Activated Tungsten Inert Gas (A-TIG) welding

By

13MMCM11

DEPARTMENT OF MECHANICAL ENGINEERING

INSTITUTE OF TECHNOLOGY

NIRMA UNIVERSITY

AHMEDABAD-382481

May 2015

Experimental studies on Activated Tungsten Inert Gas (A-TIG) welding

Major Project

Submitted in partial fulfillment of the requirements

For the degree of

Master of Technology in Mechanical Engineering

CIM

By

Sunil Bachani

13MMCM11

DEPARTMENT OF MECHANICAL ENGINEERING

INSTITUTE OF TECHNOLOGY

NIRMA UNIVERSITY

AHMEDABAD-382481

May 2015

Declaration

This is to certify that

I. The thesis comprises my original work towards the degree of Master of Technology in Mechanical Engineering (CIM) at Nirma University and has not been submitted elsewhere for Degree.
II. Due Acknowledgment has been made in the text to all other material used.

-Sunil Bachani
13MMCM11

Undertaking for Originality of the Work

I, Sunil Bachani, Roll No.13MMCM11, give undertaking that the Major Project en-titled “Experimental studies of Activated tungsten Inert gas (A-TIG) welding" submitted by me, towards the partial fulfillment of the requirements for the degree of Master of Technology in Mechanical Engineering (CIM) of Nirma University, Ahmedabad, is the original work carried out by me and I give assurance that no attempt of plagiarism has been made. I understand that in the event of any similarity found subsequently with any published work or any dissertation work elsewhere; it will result in serve disciplinary action.

_____

(Signature of Student)

Date: _____

Place: NU, Ahmedabad

Endorsed By

_____

(Signature of Guide)

Certificate

This is to certify that the Major Project entitled "Experimental Studies of Activated Tungsten Inert Gas (A-TIG) Welding" submitted by Mr. Sunil Bachani (Roll No: 13MMCM11), towards the partial fulfillment of the requirement for the degree of Master of Technology in mechanical Engineering (CIM) of Institute of Nirma university, Ahmedabad is the record of work carried out by him under my supervision and guidance. In my opinion, the submitted work has reached a level required for being accepted for examination. The result embodied in this major project, to the best of my knowledge, haven't been submitted to any other university or institution for award of any degree or diploma.

Prof. N D Ghetiya
Guide, Assistant Professor,
Department of Mechanical Engineering
Institute of Technology,
Nirma University,
Ahmedabad-382481

Dr. R N Patel
Head and Professor,
Department of Mechanical Engineering
Institute of Technology,
Nirma University,
Ahmedabad-382481

Dr. K Kotecha
Director,
Institute of Technology,
Nirma University,
Ahmedabad-382481

Acknowledgements

I want to show my gratitude to those who have helped me throughout my project work and presentations.

First of all, I would like to thank my internal project Guide Prof. N D Ghetiya our PG coordinator Prof. B M Modi & Head of Department Dr R N Patel for providing valuable guidance.

I would also like to thank our Director Dr K Kotecha for providing opportunity to work on this problem and also to the management of Nirma Education and Research Foundation (NERF) for providing enough budgets for this project work and also for providing excellent infrastructure facilities and facilities whenever and wherever required.

I am especially thankful to Mr. Ishwarbhai Patel and Mr. Jaswant Raval other workshop staff member for their technical assistance during this project work.

Finally, I am thankful to all the faculty members of Mechanical Engineering Department, Laboratory assistants, Library staff and all my friends, colleagues who have directly or indirectly helped me during this project work.

Sunil Bachani

13MMCM11

Abstract

Tungsten Inert Gas Welding (TIG) is welding process which is used in those applications requiring a high degree of quality and accuracy. However, this welding process has disadvantage of less productivity. To overcome this disadvantage Activated Tungsten Inert Gas (A-TIG) Welding is found. Experiments were performed on 304L stainless steel plates using A-TIG welding process. TIG welding fixture was designed and developed for getting fixed arc length and different welding speed. Different kinds of fluxes, TiO_2, SiO_2, CaO, MnO_2 and Al_2O_3 were used to investigate the effect of A-TIG welding process on weld geometric characteristic and distortion of weldments. A-TIG welding was carried out with different process parameters are used like welding current (60-140 A), speed (100-150 mm/min), arc gap (2 mm), gas flow rate (10 L/min), tip angle (75 degree), electro diameter (4 mm). Inverted Optical microscope with image analyzer was used to capture microstructure of weldment. A-TIG welding process parameters optimization was performed by multiobjective optimization technique named as Gray Principal Component Analysis (G-PCA). The optimum process parameters were found to be 140 A current, 100 mm/min speed and mixture of SiO_2 and TiO_2 flux.

Keywords:-TIG and A-TIG welding, TIG welding fixture, G-PCA.

Chapter 1: Introduction

1.1 Introduction

The Tungsten Inert Gas (TIG) welding process (or GTAW) is used when a good weld appearance and a high quality of the weld are required. An electric arc is formed between a tungsten electrode and the base metal in this process. The arc region is protected by an inert gas or mixture of gases. The tungsten electrode is heated to temperatures high enough for the emission of the necessary electrons for the operation of the arc. The maximum thickness of 3 mm for stainless steel is restricted to joint with this process. It is used with argon as shielding gas and low welding speed. The welding speed can be increased substantially (up to 160%) when helium or hydrogen is used as part of the shielding gas mixture. It can be increased bead penetration of the weld. Argon and helium are used as the mixture of shielding gas to improve the penetration of weld. The plasma arc welding process can be used as an alternative to the TIG process. It is allowing the welding of a 10 mm thick joint in only one pass. Plasma welding is much more complex and presents greater initial and operational costs than that for the TIG process.

The main drawbacks of TIG welding are

1. Its relatively shallow penetration capability in single passes welding operations
2. The high sensibility of the weld bead shapes to variations of the chemical composition of the base metal.
3. Its low productivity.

A variant of conventional TIG welding called Activated Tungsten Inert Gas (A-TIG) welding. A-TIG welding process is found to overcome the limitations of conventional TIG welding process. It is developed (in the 1960s) for the welding of different alloys of titanium and stainless steel. TIG welding with CaO, Fe_2O_3, and SiO_2 fluxes is used. This indicated that the surface appearance of TIG welds was produced with oxide base flux formed residual slag. Penetration and depth to width ratio is increased. It was also found that angular distortion is decreased while using SiO_2 flux in TIG welding [1]. Ming et al. [2] reported that arc voltage was increased while using SiO_2 flux and there was no any change occurred usingTiO_2 flux in TIG welding. High speed camera and oscillograph were used to capture images of arc shape during welding process.

It was also seen that arc shape was changed in A-TIG welding compared than convection TIG welding. Arc shrinkage was main aspect to increased penetration depth in A-TIG welding.

Oxide based flux powder mixed with methanol and ethanol provided good spreadability and convertibility. Smooth and clean surface were achieved by using oxide base flux. The penetration depth and bead width were increased using different values of current. It was also found that there was reduction of the angular distortion using weld parameters [3, 15]. New simplified A-TIG welding technique named as Cap Activated Tungsten Inert Gas (CA-TIG) welding used atmospheric oxygen. Simple nozzle was used to control oxygen content that increased penetration depth of weld metal. The penetration depth of weld metal was affected by the oxygen content. It was increased by the Marangoni convection with oxygen content range of 75-160 ppm [4, 10].

Flux powder was mixed with carrier solvent. It has the critical function in increasing the penetration depth of A-TIG welds. Although, several mechanism has been reasoned that increased weld penetration in A-TIG welding. It was also found that flux formulation for activated TIG welding was rare. Moreover, the new formulation that had been identified was complex [9]. A-TIG process can also used for duplex stainless steel. Thickness of 6 mm can be welded in a single pass with the ATIG process. Fine layer of flux was applied on the surface of the base metal in this process. It was indicated that penetration depth was increased up to 200-300%. It was controlled by welding parameters and must be optimized by using desirable optimize technique. Taguchi orthogonal array and Analysis of Variance (ANNOVA) techniques were used to optimize it. The optimum parameters were found to be 1 mm electrode gap, 130 mm/min welding speed, 140 A and 12 V voltage [5, 16].

Berthier et al. [6] reported effect of different activating fluxes in TIG welds. The surface tension gradient was negative and convection movements were centrifugal while using TIG welding process. An inversion current was found due to oxygen content in activating fluxes at the melting zone surface. Surface tension gradient was positive and convection movements were centripetal due to the same case. It was found that penetration depth was increased due to Marangoni effect and arc constriction effect (shown in Fig 1.1). A 2D axial symmetric model of heat transfer and fluid flow was also developed to describe Marangoni convection combined with Lorentz force in the weld metal [8].

Higher thickness of plates can be welded by single pass in A-TIG welding without filler metal. The penetration depth was got higher at lower cost. The creep tests were carried out on the base metal at 923 K over stress range of 160-280 MPa. Extensometer with dial gauge was used to monitor the elongation of base metal. The result was indicated that creep rupture was got higher strength in A-TIG more than Multi pass TIG welding process [7]. In A-TIG welding process, the arc constriction and reversed Marangoni convection were two main mechanisms increased the penetration depth. Nimonic 263 was used to base metal. The heat of the arc melted and vaporizes part of this flux during welding process. The penetration of the weld bead was increased greatly [11].

Modified P91 steel was used as weld metal in A-TIG welding process. Experimental result was found that toughness of weld metal was got low in this process. Post Weld Heat Treatment (PWHT) was required to improve toughness of weld metal. It was found that the weld metal had higher toughness after heat treatment at 760^0 C for 3 hours [12]. Iron based mix powder was used as activated flux in A-TIG welding process. TIG and A-TIG welding process were carried out on the base metal and result was found that surface discontinuous was decreased and distortion was also decreased. It was also found that penetration and depth to width ratio was increased while using mixture of FeS and FeF_2 flux [13, 18]. Low Activation Ferrite Martensitic (LAFM) steel was used as base metal. Activated flux was developed for LAFM steel material. Optical and Scanning Electron Microscopy (SEM) used to observed the characterizing the microstructures. Tensile and impact toughness tests were carried out on weld metal. This result indicated that the value of mechanical properties was obtained high in A-TIG welding process [14].

1.2 Advantages of ATIG welding process

1. It can be used for higher thickness plates with higher welding speed and reduces heat input in single pass welding.
2. Residual stresses are reduced (more than 70%) compare to conventional TIG welding process.
3. The creep rupture life is improved (more then 75%).
4. It increases productivity and decreases the cost of fabrication.
5. It can be welded up to 25 mm plates using double side welding procedure with square edge penetration.

6. Penetration increases and width of weld decreases in single pass welding.

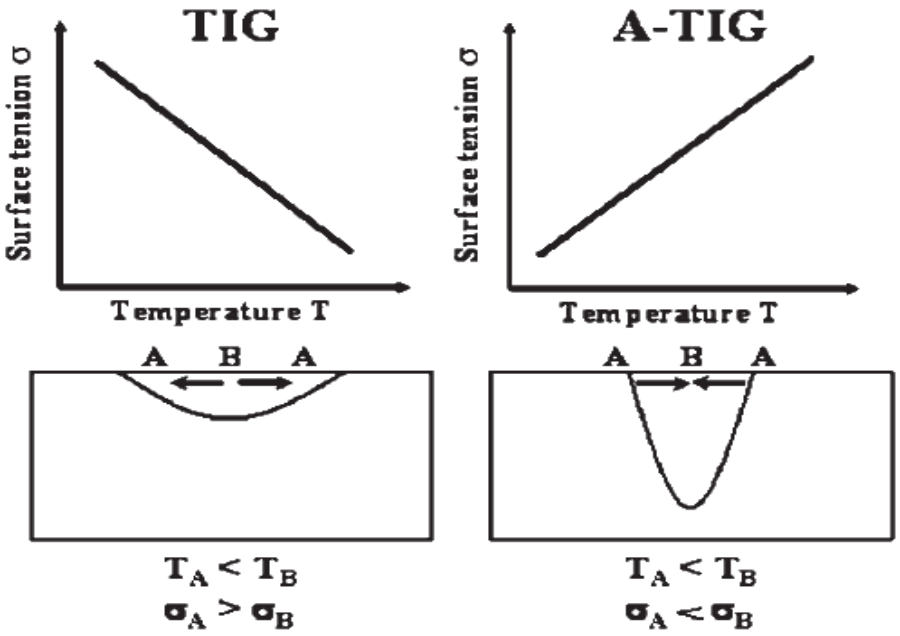

Figure 1.1-Effect of flux on weld: Marangoni effect [6]

1.3 Objective of present work

The main objectives of present study are:

1. Parametric optimization for weld bead penetration, bead width and angular distortion in A-TIG using Grey Principal Component Analysis (G-PCA).
2. Microstructure comparison between TIG and A-TIG welding process.

1.4 Methodology

The procedure described below has been used to obtain the objective:

a) Experimental set up

- Fixture design and development which is used to secure weld plate in position during welding.
- TIG welding machine is used which is available in our institute.

b) Experimental investigation

- Activated TIG welding process is used for Stainless steel 304L with 6 mm thickness as a base metal.
- Various kinds of fluxes and combination of input parameters are used in A-TIG and TIG welding process.

- After welding the surface morphology and cross section of weld bead is etched by etching solution.
- Tool Maker Microscope is used to measure penetration depth and width of weld.
- Inverted Optical Microscope with image analyzer is used to examine the microstructure of TIG and A-TIG weldments.

c) Process parameter optimization

- Optimization of process parameters for penetration depth, width and angular distortion in A-TIG welding process using optimization technique.

Chapter 2: Literature review

2.1 Literature review

Chou et al. [1] investigated effect of oxide flux on surface appearance with using activated TIG process. G3131 ms and SUS 316L SS plates of 6 mm thick was used as bas plate. It was roughly polished with 400 grit silicon carbide paper to remove surface contamination and then cleaned with acetone. The powder form of CaO, fe_2O_3, and SiO_2 fluxes were used. A thin layer flux was brushed on the surface of the joint to be welded with density was 5 to 6 mg/cm^2. ATIG process was performed on the base metal using travel speed and weld current were 150 mm/min and 200 A respectively. It was concluded using of TiO_2 and SiO_2 were increased joint penetration and weld depth to width ratio. It was also found that there was reduction in angular distortion of weld using both fluxes. Narrow and deep morphology was produced while using both fluxes.

Ming et al. [2] evaluated the effect of activating flux on arc shape and arc voltage in ATIG welding process. A special set of water cooling system and stainless steel were used as base metal for avoiding the melting of parent material during welding. The base metal was polished using 240 grit abrasive papers and cleaned by acetone. SiO_2 or TiO_2 was applied on the surface of base metal to be welded using brush. Shielding gas and cooling water were provided firstly and then the experiment was carried out by using welding currents varies from 80 to 180A and arc length was kept constant. Tip of tungsten electrode was grinded frequently using grind wheel for maintain the same electrode tip angle. Oscillograph was used to record arc voltages and arc shape was captured by high speed camera system. It was concluded that arc shape was increased with using SiO_2 flux but no any evidence was found with using TiO_2 flux. It was also found that arc voltage was increased with increasing current using of SiO_2 flux. Penetration depth was increased using both fluxes.

Tseng et al. [3] conducted the experimental study for development and application of oxide based flux powder and carrier solvent composition in ATIG welding process. Austenitic 316L S.S and balance Fe was used as base metal of 6mm thickness. It was roughly grinded with 240 grit silicon carbide abrasive paper and cleaned with acetone prior to welding. Oxide base flux was made with different fluxes and then mixed with carrier solvent to form paint and applied surface

on base metal. The specimens were prepared by sectioning, mounting, grinding and polished to 0.3 µm by etching in an electrolyte solution of 10 g oxalic acid 100 ml water for metallographic examination. The surface appearance and geometric shape of the welds were photographed with a stereo microscope. The experiment was carried out and then result show that oxide based flux powder mixed with methanol and ethanol provided good spreadability and convertibility. Smooth and clean surface were achieved by using oxide base flux. It was concluded that the penetration depth and bead width were increased using different values of current. It was also found that reduced the angular distortion using weld parameters.

Morisada et al. [4] evaluated the development and simplified active flux in TIG welding for deep penetration. SUS304 S.S of 10 mm thick plate was carried out for welding. Low sulfur content was chosen to reduce the effect of sulfur on the penetration. Specimens were prepared by sectioning and polished paste by electrolytic etching with 2mass% of oxalic acid solutions. New technique was used named as cap active flux TIG welding with atmospheric oxygen was proposed to increase the penetration depth of a weld. Nozzle cap with an air inlet was changed by the oxygen content in the molten pool. It was easily controlled by the nozzle cap and welding parameters. Stereo microscope was used to observation of cross section for the weld shape. It was concluded that the oxygen content was decreased with increasing gas flow rate. It was controlled by nozzle cap and shielding gas flow rate. The penetration depth was increased by using helium as shielding gas in increasing order.

Harikannan et al. [5] presented the optimization of process parameters in activated TIG welding. S32205 DSS of 6 mm thick plate was used as base metal. The experiment was carried out using typical branded flux: (Ador A- TIG flux- 1). It was prepared by different kinds of inorganic oxide material which change the surface activity and primarily reduce the heat energy required for penetration. The specimens were polished using different grades of emery papers and clean with diamond compound. It was etched with 10% NaOH at 2-3 V and 6-10 V by using electrolytic etching method. Macro examination was measured by stereo microscope and ferrite content was carried out by using ferritscope. The parameters of ATIG welding for aspect ratio were optimized by using Taguchi orthogonal array experimental design and other statistical tools such as analysis of variance pooled ANOVA techniques. The S/N ratio was evaluated by Taguchi method. It was represented as the desirable and undesirable values for the output characteristics. It was concluded that the electrode gap was affects the aspect ratio. The optimum parameters were

found to be electrode gap of 1 mm, travel speed of 130 mm/min, current of 140 A and voltage of 12 V. The different range of aspect ratio was acceptable range which was optimized by using method. No any evidence of solidification cracking was found by using optimized method.

Bertheir et al. [6] investigated the influences of addition of an activating flux in TIG welding. Austenitic stainless steel 304L of 4 mm thick plate was used as base metal. The mixture of TiO_2, Cr_2O_3, V_2O_5, MgF_2, and MgCl2 were used as activated fluxes. The cross section of weld bead was polished and electro etched using oxalic acid. High speed of camera was used to monitor the shape of plasma. A 2D axial symmetric model was developed to simulate the flow behavior in the melting pool. A cylindrical plate was made for simulation at initial temperature of 300 K. The molten material was isotropic, homogeneous, incompressible and Newtonian. The fluid flow was supposed to be laminar and driven by Marangoni, buoyancy and Lorentz forces. The model was used to study the influence of Marangoni effect and its inversion on the weld pool shape. It was concluded that inversion of tension gradient surface was seen of the weld bead while using the fluxes.

Bhaduri et al. [7] investigated the mechanism of creep rupture strength of weld joint in A-TIG welding process. 316L (N) SS plate of 6 mm thickness was used as base plate. A thin coating of fluxes was applied on the surface of base metal. The creep tests were carried out on base metal and cross weld joint at 923 K temperature over stress ranges of 160-280 MPa. Extensometer was used to monitor the elongation of base metal with attachment of digital dial gauge. Creep deformation was studied by creep tests at periodic intervals. Vickers hardness measurement and ferrite measurement by ferritscope were carried out on the joints. The experiment was carried out and found that the columnar grain and δ-ferrite were oriented nearly transverse to welding direction in the A-TIG weld joint. It was also found that the columnar grain and δ-ferrite were oriented nearly towards short transverse to welding direction in multi pass TIG weld joint. The equiaxed grains was grow parallel to welding direction at central location of weld metal in A-TIG process. Discontinues formation of columnar and equiaxed grains were observed in multi pass-TIG process. It was concluded that higher creep rapture strength was found in A-TIG joint than multi pass-TIG joint. Less creep cavitations was observed in A-TIG joint than multi pass TIG joint.

Ahmadi et al. [8] presented the effect of activated flux in TIG welding. 304L austenitic stainless steel of 6 mm thick plate was used as base material. 400 grit silicon carbide abrasive papers was

used to remove impurities of base plate and then cleaned by acetone. Powder form of SiO_2 and TiO_2 were used as flux. It was applied on surface of weld joint. Plate was etched by solution of 10 g $CuSO_4$ + 50 ml HCl + 50 ml H_2O with etching process. Optical microscope was used to photograph of cross section of weld bead. A 2D axial symmetric model was developed to simulate the flow of behavior in melting pool. It was concluded that penetration depth was increased while using both fluxes. It was also found that width of weld bead was decreased. Delta ferrite content of weld metal was increased in ATIG welding process. Mechanical properties of weld metal were also improved while using ATIG welding process.

Pereira et al. [9] evaluated the use of active fluxes in ATIG welding process. AISI 304 austenitic steel plates with thickness of 5-8 mm were used as base material. It was straightened and cleaned with acetone. The mixing of AlF_3, Al_2O_3, Cr_3O_3, CaF_2, Fe_2O_3, NaF, Na_2WO_4, SiO_2, and TiO_2 was used as flux. It was applied on the surface of base metal before welding. Digital data acquisition system was used to record arc current and voltage in every 10 second. CCD camera was used to capture images of the electric arc. The cross section of plate was etched with solution of cupric chloride. It was used to observe profile projector, measure the penetration and width of the weld. It was concluded that the radish arc was found while using NaF flux. Electric arc was deflected forward direction while using SiO_2 flux. The penetration depth was increased with using the fluxes of AlF_3, Cr_3O_3, SiO_2 and TiO_2.

Nogi et al. [10] presented the effect of active flux on the Marangoni convection in ATIG welding. SUS304 stainless steel plate of 10 mm thickness was used as base metal. Cu_2O, NiO, Cr_2O_3, SiO_2 and TiO_2 were used as activated fluxes. It was applied on the surface of base metal. The cross section plate was etched by solution of HCl+Cu_2SO_4. Optical microscope was used to photograph of surface morphology and cross section of bead. Oxygen analyzer was used to measure oxygen content of weld metal. It was conclude that penetration depth was increased but it was decreased with increased Cu_2O, NiO, Cr_2O_3 and SiO_2 fluxes. The depth to width ratio was increased with oxygen content in the range of 70-300 ppm. Marangoni convection was seen weak with increased oxygen content of weld plate. It was also found that maximum penetration depth was seen while using TiO_2 flux.

Y.L.Xu et al. [11] investigated Marangoni and weld shape variation of weld metal in ATIG welding process. Nimonic 263 specimens were used as base metal. It was polished and clean with acetone. TiO, TiO_2, and Ti_2O_3 were used as fluxes. It was prepared with mixer of oxides

fluxes with acetone. It was applied on the half surface of weld bead. Experiment was carried out by both TIG and A-TIG welding process with same parameters. It was concluded that the arc constriction and the reversed Marangoni convection were considered for increasing penetration of A-TIG weld pool. Penetration depth was increased with increased fluxes with critical value but it was decreased with more than critical value. The width of weld pool was gotten deep and narrow with positive surface tension temperature coefficient above 2000 K. Oxygen content was affected the changed of weld shapes.

Vasudevan et al. [12] investigated microstructure and impact toughness of weld metal in A-TIG and TIG welding process. P91 steel plate of 12 mm thickness was used as base metal. The mixture of SiO_2 and TiO_2 was used as activated flux. It was applied manually as a paste on the surface of weld metal. Preheating was carried out using oxy acetylene natural flame at temperature range of 200 to 250^0 C during welding. Welding was carried out using fully automated A-TIG and TIG process set-up in flat (1G) position. X-ray radiography was used to evaluate the joint of weldment. Post weld heat treatment (PWHT) was carried out at 760^0 C with time varied of 2-3 h. It was used to improve the toughness of weldment. Base metal was etched using Villella's etchant (1g picric acid+5ml HCl+100ml ethanol) for micro structural observation. Transmission Electron Microscope (TEM) was used to observed microstructure of weldment. Charpy test was carried out in order to evaluate the absorbed energy of weldment at room temperature. Scanning Electron Microscope (SEM) was used to fractograph of broken Charpy impact specimens. Thermo Calc Windows (TCW) was used to evaluate the equilibrium critical phase transformation points in A-TIG and TIG welding process. It was conclude that the TIG weld was higher toughness than A-TIG weld. It was also found that A-TIG weld was required prolonged post weld heat treatment at 760^0 C for 2h. A-TIG weld was improved toughness after carried out PWHT at 760^0 C for 3h.

Chuang et al. [13] reported the influence of the flux powders in TIG welding. Austenitic 316L stainless steel with 5mm thickness was used as base metal. Powder form of FeF_2, FeO, and FeS were used in as flux. It was mixed with carrier solvent and applied on the surface of base metal. Charge Couple Device (CCD) system was used to observe and record the image of arc profile during welding. The Varestraint (variable restraint) test was carried out for evaluated the alloy's susceptibility to forming hot crack during welding. Vickers hardness test was carried out for examined the changes in mechanical properties and metallurgical structures of weld metal.

Stereomicroscope was used to photograph of surface appearance and geometric shape of weld metal. Optical microscopy and scanning electron microscopy were used to evaluate metallurgical characterization. It was concluded that surface appearance was produced good while using FeF_2 flux but slag and spatter were produced while using FeS and FeO fluxes. Penetration depth and weld aspect ratio were increased and angular distortion and hot crack susceptibility were reduced while using FeS and FeO fluxes. It was also found that maximum penetration depth was got while using FeO flux.

Vasudevan et al. [14] studied of low activation Ferritic/Martensitic steel in A-TIG welding. LAFM steel was used as base metal in A-TIG welding process. Fluxes were mixed with acetone and applied on the surface of base metal using paint brush. Post weld heat treatment (PWHT) was carried out for 4 hour at 760^0 C. It was etched with Villella reagent (1g picric acid+5ml HCl+100ml ethanol) for metallographic studies. Optical microscope and Scanning Electron Microscope (SEM) were used to observe microstructures of weld joints before and after PWHT. Mechanical properties were evaluated by Tensile and Charpy tests of weld joints. Impact tests were also carried out of weld joints. It was concluded that penetration depth was increased and bead width was decreased with same parameters in A-TIG welding process than TIG welding process. It was also indicated that coarse and harder Martensitic was observed in fusion zone and HAZ of the weld joints. Joint properties were improved by Post Weld Heat Treatment process. It was observed that the grain size of base metal was smaller than weld metal. A-TIG weld joint was stronger than base metal.

Tseng et al. [15] investigated the effect of activated TIG process in austenitic stainless steel. 316L stainless steel was used as base metal in A-TIG welding process. Powder form of MnO_2, SiO_2, MoO_3, TiO_2 and Al_2O_3 were used as activated flux. It was mixed with acetone and applied on the surface of base metal as paste form using paint brush. The experiments were carried out with and without activated fluxes at electrode diameter of 2.4 and 3.2 mm. Charge Couple Device (CCD) was used to observe and record the image of the weld arc during welding process. Digital video recorder system was used to monitor the arc voltage. The fisher maker ferritscope was used to measure delta ferrite content of weld metal and base material. Metallurgical properties of weld metal were examined by microhardness test. It was etched by solution of 10 g $CuSO_4$ + 50 ml HCl + 50 ml H_2O with etching process. Weld depth and bead width were measured by Optical Microscope. It was concluded that arc voltage was increased when A-TIG

welding process was used. It was also found that the oxide base flux was acted as high electric insulators. The result was indicated that activated TIG arc voltage was produced by 2.4 mm electrode unstable compared than 3.2 mm electrode. It was also seen that penetration depth was increased and bead width was decreased while using SiO_2, MoO_3 fluxes. It was also concluded that penetration depth was increased by surface tension gradient and plasma arc column of A-TIG joint. It was also found that distortion angle was increased while using activated fluxes.

Tsai et al. [16] reported the effects of activated fluxes on duplex stainless steel in tungsten inert gas welding process. 2205 stainless steel plate was used as base metal. MnO_2, SiO_2, MoO_3, TiO_2 and Cr_2O_3 were used as activated flux. It was mixed with acetone as paste form and applied on the surface of base metal. Charge Couple Device (CCD) detector was used to record images of weld arc during welding process. The mean vertical displacement method was used to measure the distortion of weld metal. Ferritscope was used to measure ferrite content of base metal. Tensile test was also carried out for the metallurgical properties of weld metal. Scanning Electron Microscope (SEM) was used to observe tensile fracture mode of weld metal. It was etched by Kalling's solution with etching process. Optical microscope was used to measure of penetration depth and bead width of weld metal. It was concluded that smooth and clean surface was produced while using fluxes. It was also found that excessive residual slag was produced while using TiO_2 and Cr_2O_3 flux. The results were indicated that the penetration depth was got high while using SiO_2 flux. Narrow and deep morphology was produced while using fluxes. It was also found that distortion angle was increased while using activated fluxes. Weld depth to width ratio and joint penetration were increased while using activated fluxes. Delta ferrite content of weld metal was decreased in activated TIG process. It was also found that a mechanical property was improved while using Cr_2O_3, SiO_2, MoO_3 fluxes.

Marya et al. [17] investigated the effect of coating geometry and thickness on weld penetration. AISI304L stainless steel was used as base metal. Silica powder was used as activated flux. It was mixed with liquid carrier solvent to form of paste and applied on the surface of base metal. Experiments were carried out A-TIG and Flux Bounded TIG (FB) process. It was etched with nitric acid by etching process. Tensile test was also carried out in weld metal. Macro examination was measured by stereo microscope. CCD camera was used to record the images of arc voltage during welding process. It was concluded that penetration depth was increased up to 200 µm thickness of coating in FB-TIG welding process but it was increased up to 70 µm thickness of

coating in A-TIG process. It was also found that penetration depth was increased with increased coating thickness in FB-TIG welding process. It was also found that tensile strength was reduced than TIG welding process.

Wang et al. [18] evaluated to improve joint penetration and weld quality in A-TIG welding process. 316L stainless steel was used as base metal. The powder form of FeS and FeF_2 were used as activated flux. It was mixed with methanol as paste form and applied on the surface of base metal using paint brush. Charge couple device was used to record images of arc profile during welding process. It was etched with solution of 10 g oxalic acid + 100 ml water by electrolyte etching process. Surface appearance and weld shape were observed by Stereo microscope. It was concluded that clean and smooth surface was appeared while using ionic compound in TIG welding process. It was also found that surface discontinues was decreased with increasing the concentration of FeS/FeF_2 mixture. Penetration was increased while using the same. The width and depth ratio was increased while using 75% FeS and 25% FeF_2.

Badheka et al. [19] studied the effect of activating fluxes on mechanical and metallurgical properties of dissimilar activated flux-TIG welding process. Gr70 Carbon steel and 304 stainless steel was used as base metal. Powder form of TiO_2, ZaO and MnO_2 were used as activated flux. It is mixed with acetone as paste form and manually applied on the surface of base metal. Experiments were carried out by both TIG and A-TIG welding process. It was etched by 5% nital by etching process. Traveling microscope was used to measure bead width and bead depth. It was concluded that penetration was got maximum while using TiO_2, ZaO fluxes. It was also found that depth and width ratio was increased while using same. Lowest angular distortion was found while using TiO_2 fluxes.

2.2 Summary

Following is summary of literature review.

- A-TIG welding process is used to weld thickness of 6 to 10 mm stainless steel.
- Penetration depth is increased up to 200% than conventional TIG welding with using different kind of fluxes in ATIG welding process.
- There are various process parameters affecting in ATIG welding like welding current, speed, rate of shielding gas, voltage, and tip angle. Table 2.1 shows research work done on these A-TIG welding process parameters.

- The microstructure in various regions of the welded plates is observed by Optical Microscope and Tool maker microscope.
- The creep rapture life is improved by using activated fluxes in ATIG welding process.
- For the measurement of arc length during welding process the high speed camera is at various positions and then captured the images of arc length.
- The distortion angle and width of weld bead is decreased with using different kind of fluxes in ATIG welding process.
- The arc constriction and reversed Marangoni convection are considered to be the two main mechanisms contributing to increasing penetration during A-TIG welding.

.

Table 2.1 Important process parameters of A-TIG welding

Author	Material used	Fluxes	Input Parameter
Chou et al. [1]	G3131 ms and SUS 316L SS	CaO, fe2O3, and SiO2	Travel speed (150 mm/min), weld current (200A) and gas flow rate (12 L/min)
Ming et al. [2]	stainless steel	SiO2 and TiO2	welding current (80-180 A), gas flow rate (9 L/min) and welding speed (175 mm/min), Electrode diameter (2.4 mm), Tip angle (45^o), Arc length (3 mm)
Tseng et al. [3]	Austenitic 316L SS	(SiO_2- 30wt%, TiO_2- 25wt%, Cr_2O_3- 25wt%, MoO_3- 10wt%, NiF_2- 5wt%, MoS_2- 5wt%)	welding current (80-180 A), gas flow rate (9 L/min) and welding speed (175 mm/min), Electrode diameter (2.4 mm), Tip angle (45^o), Arc length (3 mm)
Morisada et al. [4]	SUS 304 S.S	SiO2, Cr2O3, MoO3	welding current (180 A), gas flow rate (1 to 20 L/min) and welding speed (120 mm/min), vertex angle (60^o), Arc length (3 mm)
Harikannan et al. [5]	S32205 DSS	Ador A TIG flux	Electrode gap (1,2,3 mm), Travel speed (100,115,130 mm/min, Voltage (12,14,16.5 V), current (120,140,160 A)
Bertheir et al. [6]	stainless steel 304L	TiO2, Cr2O3, V2O5, MgF2 and MgCl2.TiO2, Cr2O3, K2Cr2O7 and MgF2	current (100A), voltage (10V), arc efficiency (75%), heat distribution (1.6mm)
Bhaduri et al. [7]	316L S.S	SiO_2, TiO_2	welding current (200A), welding speed (120mm/min),voltage (12.5 V), Heat input (1250 KJ/mm),

			temperature (923 K), stress (160-280 MPa)
Ahmadi et al. [8]	stainless steel 304L	SiO_2, TiO_2	welding current (180 A), gas flow rate (13 L/min), welding speed (150 mm/min), Electrode diameter (3.2 mm), Tip angle (75^o), Arc length (3 mm)
Pereira et al. [9]	AISI 304 austenitic steel	AlF3, Al2O3, Cr3O3, CaF2, Fe2O3, NaF, Na2WO4, SiO2, and TiO2	welding current (200-300 A), gas flow rate (10 L/min), welding speed (200 mm/min), Electrode diameter (3.2 mm, W-2% ThO), Tip angle (60^o), Arc length (1-3 mm), Bead length (100-120 mm)
Nogi et al. [10]	SUS304 stainless steel	Cu2O, NiO, Cr2O3, SiO2 and TiO2	welding current (80 and 160 A), gas flow rate (10 L/min), welding speed (120 mm/min), Electrode diameter (1.6 mm), Tip angle (60^o), Arc length (3 mm), Bead length (50 mm)
Y.L.Xu et al. [11]	Nimonic 263	TiO, TiO2, Ti2O3	welding speed (1.5 mm/sec), Bead length (90 mm),welding current (150 A), voltage (10 V), coating density 0.6-6 mg/cm2)
Vasudevan et al. [12]	P91 steel	SiO_2, TiO_2	Tip angle (60^o), Gas flow rate (10 L/min),Heat input (0.8 & 1.04 Kj/mm)
Chuang et al. [13]	Austenitic 316L SS	FeF2, FeO, and FeS	Tip angle (45^o), Electrode diameter (2mm), Current (100A), Arc length (1.6mm)
Vasudevan et al. [14]	Low Activation Ferritic- Martensitic		Current (100-280 A), Travel Speed (120 mm/min), Voltage (14.7 V), Arc

	(LAFM) steel		gap (1 mm), Gas flow rate (10 L/min), Preheat Temp. (250^{o}C)
Tseng et al. [15]	Austenitic 316L SS	MnO_2, SiO_2, MoO_3, TiO_2 and Al_2O_3	Current (200 A), Travel Speed (150 mm/min), Voltage (14.7 V), Arc gap (2 mm), Gas flow rate (10 L/min), Tip angle (45^{o}), Electrode diameter (2.4 & 3.2mm)
Tsai et al. [16]	2205 Duplex Stainless Steel	MnO_2, SiO_2, MoO_3, TiO_2 and Cr_2O_3	Current (200 A), Travel Speed (150 mm/min), Arc gap (2 mm), Gas flow rate (10 L/min), Tip angle (45^{o}), Electrode diameter (3.2mm)
Marya et al. [17]	AISI 304L austenitic steel	Silica powder	Current (100-125-150 A), Travel Speed (125 mm/min), Arc gap (2 mm), Gas flow rate (12 L/min), Tip angle (60^{o}), Electrode diameter (2.4mm), Bead length (100-130 mm)
Wang et al. [18]	Austenitic 316L SS	FeF2, and FeS	Current (180 A), Travel Speed (160 mm/min), Arc gap (3 mm), Gas flow rate (12 L/min), Tip angle (45^{o}), Electrode diameter (3.2mm)
Badheka et al. [19]	stainless steel 304 and Gr70 carbon steel	TiO2, MnO2, ZnO	Current (200 A), Travel Speed (55 mm/min), Arc gap (2 mm), Gas flow rate (12 L/min), Tip angle (60^{o}), Electrode diameter (3 mm), Root Gap (1.5 mm)

Chapter 3: Experimental Set-up

3.1 Introduction

In A-TIG welding process, TIG welding fixture is designed and developed for achieving different welding speed and fixed arc length. The workpiece should be placed such that it can be welded without any defects. Trial experiments were carried out for selection of process parameters which results in formation of minimum visual defect.

Experimental set-up consists of:

a. TIG welding setup
b. TIG welding fixture

3.2 TIG welding set-up

Tungsten Inert Gas (TIG) welding is process that produces an electric arc between a non-consumable electrode and the workpiece. This electric arc produced by passage of current through a conductive ionized inert gas. It is also provides shielding gas to electrode, molten weld pool and solidifying metal from contamination by the atmosphere. Figure 3.1 shows TIG welding set-up which is utilized for experimental investigation. It has current range of 60-140 A.

The components of TIG welding set up are:

1. Welding Torch
2. Electrode
3. Welding power source
4. Shielding gas cylinder

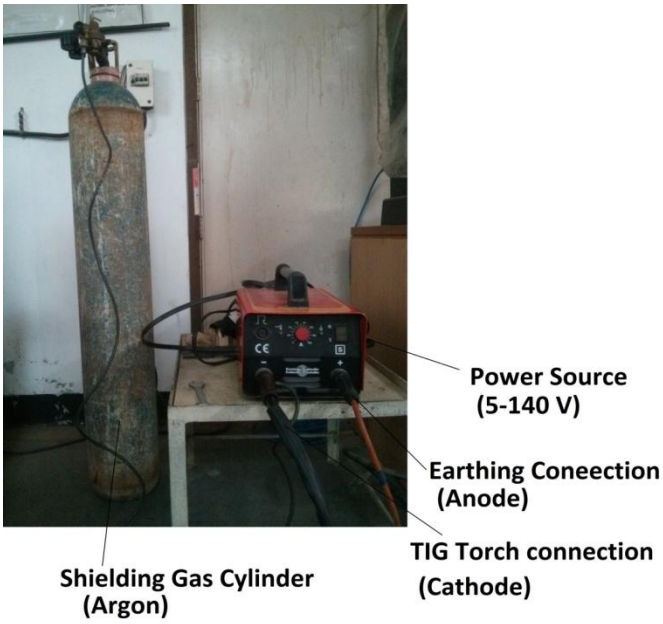

Figure 3.1: TIG welding Set-up

3.3 Process variables affecting A-TIG welding

The main process variables in TIG welding are:

I. **Arc current-** Arc current is the most effective process parameter to get deep penetration. Deep penetration and required speed are achieved while using D.C current. Alternating current is provided cathodic cleaning which can remove refractory oxide from the joint surface. It is provided high weld quality.

II. **Arc Voltage-** Arc voltage is the voltage difference between tungsten and base metal during welding. It is depended on arc current, shape of tungsten electrode tip, distance between tungsten electrode and base metal and type of shielding gas used. Arc length is controlled by arc voltage and it is affected to the weld width. Due to this reason the arc voltage is maintained low during welding process.

III. **Travel speed-** Travel speed is affected both the penetration and width of TIG weld. While using automatic welding process travel speed is very important factor and other variables like current and voltage are adjusted accordingly. In this case travel speed is depended variable along with other variables to obtain high depth to width ratio.

IV. **Activated Flux-** Activated flux is also affected the penetration depth and width of weld metal. While using activated flux, reversed Marangoni convection and arc constrictions

are two mechanisms achieved which is helped to get high depth to width ratio of weld metal and reduce the distortion of weld metal.

V. **Shielding gas-** shielding gas is used to protect the electrode and molten weld metal from the atmospheric contamination. Argon and Helium or their mixtures are the most commonly used inert gas for shielding purpose. Argon-Hydrogen mixtures are also used for some special application.

3.4 Automated TIG welding fixture

While doing manually TIG welding process, the arc length cannot be kept constant and welding speeds cannot be varied so overcome these problems the TIG welding fixture is designed and developed. It is also require to maintain constant speed of moving plate on which workpiece is put during welding. Inappropriate fixture results in deviation of speed and poor quality of welded joint. Appropriate welding speeds are maintained for producing good quality of weld joint during A-TIG welding process. Under the effect of these speeds, fixture must capable to get desired quality of welds which is shown in figure 3.2.

Figure 3.2 TIG welding fixture

3.4.1 Design

A welding fixture is a device for locating and supporting work piece during welding process. The design of welding fixture should be such that the weldment can be easily welded. In order to maintain welding speed and arc length during welding process, an operational fixture has to satisfy several requirements to fully perform its function. Figure 3.3 (a) shows TIG welding torch with fixture and (b) shows working condition of TIG welding fixture.

(a)

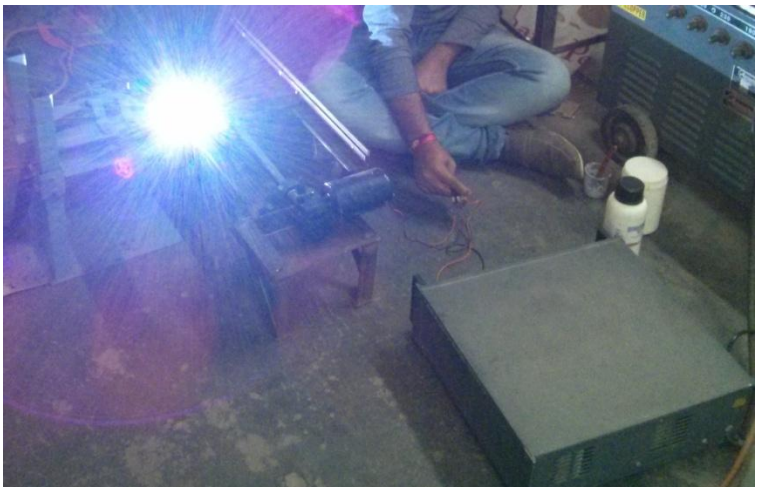

(b)

Figure 3.3 (a) TIG welding torch with fixture (b) A-TIG welding using fixture

Fixture is designed with an appropriate alignment of moving plate and fixed torch such that unique speed and good welding quality are obtained. Moving plate is not aligning properly; it may results non uniformity in the welding. To assure that the fixture components do not interface with the welding torch during A-TIG welding process.

In addition this fixture has desirable characteristics such as different welding speed and constant arc length and fully accessibility to A-TIG welding process during experiments.

3.5 Selection of workpiece material

Stainless steels are engineering materials with good corrosion-resistance, strength and fabrication characteristics. They can readily meet a wide range of design criteria, including load, service life and low maintenance. Selecting the proper stainless steel grades involves four qualities in the following order of importance:

a. Corrosion or heat resistance
b. Mechanical properties
c. Fabrication operation
d. Cost

Type 304L is an extra low-carbon variation of Type 304 with a 0.03% maximum carbon content that eliminates carbide precipitation due to welding. As a result, this alloy can be used in the "as welded" condition, even in severe corrosive conditions. In many cases it eliminates the necessity of annealing weldment except for applications specifying stress relief. Type 304L has slightly. Hence in the present work, experimental investigations are carried out to analyze the effect of

Activated TIG welding process parameters on the penetration depth and bead width of 304L stainless steel.

3.6 Selection of Process Parameters

The parameters can be classified as machine parameters, process parameters, material based parameters. It is necessary to choose a sensible set of factors to be varied in the experiments. From the literature review and trial experiments the predominant factors which are having greater manipulate on penetration depth and width of activated TIG welded stainless steel 304L is identified. They are as follow:

- Welding Current
- Welding Speed
- Welding Flux

The experiments are conducted keeping these factors at various levels. The range of each factor has been selected based on the review of past literature and preliminary experiments conducted by using one variable at a time approach.

3.7 Trial Experiments

Trial experiments are carried out to determine the working range of the process parameters and good quality of weld joints. Feasible limits of the parameters are chosen in such way that the A-TIG welded joints should be good quality. A-TIG welding of stainless steel plate with 6 mm thickness has been carried out on TIG welding fixture prepared with TIG welding machine. Welding speed available on TIG welding fixture is shown in Table 3.1.

Table 3.1 Different Speeds available in Fixture

Sr. No	Welding Speed (mm/min)
1	55
2	72
3	80

4	90
5	100
6	120
7	132
8	138
9	150
10	162
11	185

Stainless steel 304L plates of 6 mm thickness are cut into the required size (300 mm x 75 mm). The flux is prepared by mixing combination of two fluxes (TiO_2+ MnO_2) with carrier solvent. The paste form of this mixture is applied manually by paint brush on top surface of weldment just before welding. Figure 3.4 shows that trail experiments are carried out in TIG and A-TIG welding process. The total joint configuration is dived in to the 4 part to use 2 different combinations of process parameters in one trial (Shown in Table 3.2).

Table 3.2 Process parameters and their value for trial experiment

Process parameter	Value	
Welding Speed (mm/min)	160	80
Welding Current (A)	140	60

Figure 3.4 Appearance of a weld made on Stainless Steel 304L

After welding process the cross section of weldment is etched with etching solution of 10g $CuSO_4$ with 100 ml HCl. It is observed by Tool Maker's Microscope and measure penetration depth and width of weldment. The experiments result indicated that using of activated flux, the penetration depth is increased and width of weldment is decreased. The penetration depth is increased with increasing welding current and width of weldment is decreased with decreasing welding speed in A-TIG welding process. Penetration depth is higher for process parameters of 80 mm/min, 140 V and width of weldment is lower for process parameter of 60 V, 160 mm/min.

3.8 Measurement of Angular Distortion

Angular distortion is measured and method for the same is shown in 3.5. The five positions on either side of the welds are marked, and the distance from each point to the horizontal surface is then recorded. Measurements are taken before and after welding. During measurement the dial indicators is moving along X- axis direction and then mean vertical displacement of each side is obtained. The angular distortion θ can be derived from equation. Conclusively the five positions on either side of the welds are averaged, then added together to get the mean angular distortion value.

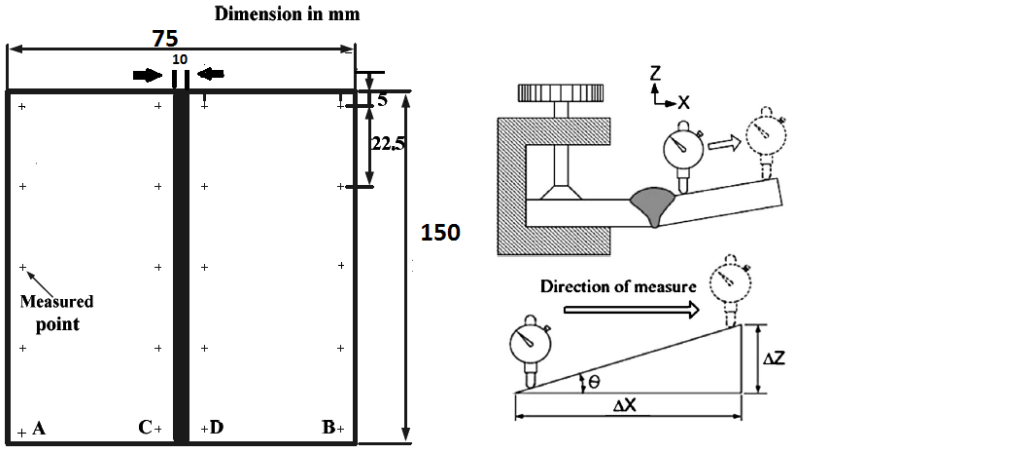

(a) Measuring Positions (b) Angular Distortion Measurement [19]

Figure 3.5 Schematic diagram of weld distortion measurement

4. Multiobjective Optimization of A-TIG Welding

4.1 Introduction

Experimental investigations are carried out to analyze the effect of A-TIG welding process parameters is order to achieve maximum penetration depth and minimum weld width and angular distortion. The objective of this chapter is to find the optimum levels of the process parameters with using the multiobjective technique known as Grey Principal Component Analysis (G-PCA).

4.2 Experimental Design

A well designed experiment can substantially decrease the number of trials. In classical methods of experimental planning a large number of experiments have to be carried out as the number of the process parameters increase which is difficult and time consuming and also results in higher cost. Taguchi design is the most preferred class of design for the experimentation. Orthogonal array L_{18} is used to conduct the experiments with three levels. Table 4.1 shows the typical plan of 18 different trials.

Table 4.1 L_{18} orthogonal array for experimentation

Trial	Current (A)	Speed (mm/min)	Flux
1	1	1	1

2	1	2	2
3	1	3	3
4	2	1	1
5	2	2	2
6	2	3	3
7	3	1	2
8	3	2	3
9	3	3	1
10	1	1	3
11	1	2	1
12	1	3	2
13	2	1	2
14	2	2	3
15	2	3	1
16	3	1	3
17	3	2	1
18	3	3	2

4.3 Experimentation

Welding was carried out on 6 mm thick stainless steel 304L plates whose chemical composition and mechanical properties are shown in Table 4.2 and Table 4.3. SS 304L plates were cut into 150 × 75 mm strips for A-TIG welding. Before welding, it was roughly polished with 240 grit carbide abrasive paper to remove surface contamination and then cleaned with acetone. Activated flux was prepared using three kinds of combination oxides (TiO_2+ MnO_2, SiO_2+ TiO_2 and Al_2O_3+ CaO) packed in powdered form. These powders were mixed with methanol to produce paint like consistency. Before welding a thin layer of the flux was applied on the surface of base metal to be welded. A-TIG experiment was carried out as per the Taguchi design. Welding fixture was designed and developed for getting fixed arc length and different welding speed. After experiments, the angular distortion was measured by vertical displacement theory.

Table 4.2 Chemical composition of Stainless Steel 304L

C	Si	Mn	P	Cr	Ni	S	N	Fe
0.03	0.75	2	0.045	18	10	0.03	0.1	Bal.

Table 4.3 Properties of Stainless Steel 304L

UTS (MPa)	Density (Kg/m^3)	Thermal Conductivity (W/m-k)	Melting Point (^{0} C)	Hardness (HRB)
586	8030	16.2	1399	82

The specimens were cut from strip with the use of power hacksaw machine for the weld bead observation and microstructure examination. All these specimen were prepared by grinding, polishing and then followed by etching in a solution of 10 g $CuSo_4$ + 50 ml HCl and swab with soft cotton for few seconds. Tool maker's microscope was used to measure the weld bead width and bead depth. Microstructure of different zones like weld metal, base metal and fusion boundary under different flux combination were viewed and captured by using inverted optical microscope coupled with image analyzer software at magnification of 500X.

Total 18 experiments have been carried out using L_{18} Orthogonal Array (OA) with process parameters variables at 3 different levels. Level of process parameters and design matrix are given in Table 4.4 and Table 4.5 respectively.

Table 4.4 Process parameters and levels

Process parameter	Unit	Level		
		Low	Medium	High
Current	A	60	100	140
Welding Speed	mm/min	100	125	150
Flux	-	TiO_2+ MnO_2 (1)	SiO_2+ TiO_2 (2)	Al_2O_3+ CaO (3)

Table 4.5 Design matrix and experiments result

Trial	Input Parameters			Responses		
	Current	Speed	Flux	Penetration	Width	Distortion
1	60	100	1	0.99	4.5	1.215
2	60	125	2	1.37	3.1	1.34
3	60	150	3	1.27	3.15	2.764
4	100	100	1	1.16	7.49	2.77
5	100	125	2	1.4	4.04	2.972
6	100	150	3	2.47	3.36	3.045
7	140	100	2	3.64	7.48	0.76
8	140	125	3	3.38	4.88	1.57
9	140	150	1	2.62	7.64	1.789
10	60	100	3	2.34	2.51	1.258

11	60	125	1	0.5	3.53	2.262
12	60	150	2	1.43	3.76	2.577
13	100	100	2	1.07	3.6	1.95
14	100	125	3	2.4	3.7	2.034
15	100	150	1	1.29	5.99	3.769
16	140	100	3	3.4	6.14	1.5
17	140	125	1	2.91	3.95	1.867
18	140	150	2	4.06	4.28	1.749

4.4 Analysis Method

4.4.1 Grey Principal Component Analysis (G-PCA)

In G-PCA, experimental results are first normalized and then the grey relational coefficient is calculated from the normalized experimental data to see the relationship between the desired and actual experimental results. Then the grey relational grade is computed by averaging the grey relational coefficient corresponding to each response. The overall evaluation of the multiple process responses is based on the grey relational grade.

Step 1- Data Processing

In the analysis of the process parameter of A-TIG welding, an appropriate mathematics model is established to study the relationship between target value and quality characteristics which is obtained by the experiment. G-PCA is measured the correlation degree among factors based on the similarity or difference among it. It involves data processing and calculation according to the quality characteristics. Calculate method of the grey relational generation is as follows:

1) The larger the better characteristic (higher the target value, the better)

$$Z_{ij} = \qquad (1)$$

2) The smaller the better characteristic (smaller the target value, the better)

$$Z_{ij} = \qquad (2)$$

3) Nominal the better characteristic (if target specify value, set target value OB)

$$Z_{ij} = 1- \qquad (3)$$

Where Z_{ij} is the sequence after data processing; Y_{ij} is original sequence of responses. Max Y_{ij} is maximum value of Y_{ij} and min Y_{ij} is minimum value of Y_{ij}.

The normalized value of responses in penetration depth, weld width and angular distortion are calculated according to the larger the better and smaller the better characteristics of sequence by

using equations (1) and (2). The normalized value can be calculated as follows and shown in Table 4.6

Z_{01} (1) =
Z_{01} (2) =
Z_{01} (3) =

Table 4.6 The normalized value

Trial	Penetration	Width	Distortion
Reference Sequence Comparability sequence	1.000	1.000	1.000
1	0.138	0.551	0.849
2	0.244	0.867	0.807
3	0.216	0.608	0.334
4	0.185	0.293	0.332
5	0.253	0.687	0.265
6	0.553	0.655	0.241
7	0.882	0.720	1
8	0.809	0.676	0.731
9	0.600	0	0.658
10	0.517	1	0.834
11	0	0.770	0.501
12	0.261	0.660	0.396
13	0.160	0.755	0.605
14	0.531	0.732	0.577
15	0.222	0.216	0
16	0.815	0.760	0.754
17	0.677	0.676	0.632
18	1	0.601	0.671

According to Table 4.6 the deviation sequences Δ_{01} can be calculated as follows:

Δ_{01} (1) = |1.000 – 0.138| = 0.862
Δ_{01} (2) = |1.000 – 0.551| = 0.449
Δ_{01} (3) = |1.000 – 0.849| = 0.151

Therefore Δ_{01} = (0.862, 0.449, 0.151). The same calculating method is performed for i=1,2,3…18 and values are listed in Table 4.7. Δ_{max} and Δ_{min} can be expressed as follows:

$\Delta_{max} = \Delta_{11}$ (1) = Δ_{09} (2) = Δ_{15} (3) = 1.000
$\Delta_{min} = \Delta_{18}$ (1) = Δ_{10} (2) = Δ_{07} (3) = 0.000

Table 4.7 Deviation sequence

Trial	Penetration	Width	Distortion
1	0.862	0.448	0.151
2	0.756	0.133	0.193
3	0.784	0.392	0.666
4	0.815	0.707	0.668
5	0.747	0.313	0.735
6	0.447	0.345	0.759
7	0.118	0.280	0
8	0.191	0.324	0.269
9	0.404	1	0.342
10	0.483	0	0.166
11	1	0.230	0.499
12	0.739	0.340	0.604
13	0.840	0.245	0.395
14	0.466	0.268	0.423
15	0.778	0.784	1
16	0.185	0.271	0.246
17	0.323	0.324	0.368
18	0	0.400	0.329

Step 2- Grey relation coefficient

It is expressed the relationship between the best and the actual normalized experimental results from the normalized S/N ratio using equation (4).

$$\mathcal{E}_i [Y_0, Y_i] = \qquad (4)$$

Where i= 1,2…n: n is the number of the trials. Δ_{0i} is deviation sequence of the reference Sequence. i.e. $\Delta_{0i} = |Y_0 - Y_i|$ is the absolute value of difference between Y_0 and Y_i. Δ_{min} is minimum value of Δ_{0i} and Δ_{max} is maximum value of Δ_{0i}.

ξ is the distinguishing coefficient whose value is taken to be 0.5 for each response to ensure the equal importance for all the responses.

The grey relational coefficient for the each quality characteristic are calculated by substituting the distinguishing coefficient $\xi = 0.5$ by using equation (4). Grey relational coefficients $\mathcal{E}_i$ are provided as follows and sown in Table 4.8.

$$\mathcal{E}_1 (1) = \ = 0.367$$
$$\mathcal{E}_1 (2) = \ = 0.448$$

$\varepsilon_1(3) = = 0.768$

Table 4.8 Grey Relational Coefficients

Trial	Penetration	Width	Distortion
1	0.367	0.527	0.768
2	0.398	0.790	0.722
3	0.389	0.561	0.429
4	0.380	0.414	0.428
5	0.400	0.615	0.405
6	0.528	0.592	0.397
7	0.809	0.642	1
8	0.724	0.607	0.650
9	0.553	0.333	0.594
10	0.509	1	0.751
11	0.333	0.985	0.500
12	0.404	0.595	0.453
13	0.373	0.971	0.558
14	0.517	0.651	0.541
15	0.391	0.389	0.333
16	0.730	0.675	0.670
17	0.608	0.607	0.576
18	1	0.559	0.603

Step 3- Principal Component Analysis (PCA)

Principal Component Analysis (PCA) explains the structure of variance covariance by the linear combinations of each quality characteristic.

1. The original multiple quality characteristic array

$$Y_i(j),\ i= 1, 2\ldots m;\ j= 1, 2\ldots n \qquad (5)$$

$$A =$$

Where m is the number of trials and n is the number of the quality characteristic. In this paper Y is the grey relational coefficient of each quality characteristic and m = 18, n = 3.

2. Correlation Coefficient Array is calculated as follow equation:

$$R_{ji} = , \quad j = 1,2\ldots n;\ l = 1,2\ldots n \qquad (6)$$

Where Cov (Y_i (j), Y_i (l) are covariance sequence $Y_{i\,(j)}$ and Y_i (l) respectively σ_{Yi} (j) is the standard deviation of sequence Y_i (j), σ_{Yi} (l) is the standard deviation of sequence Y_i (l).

3. Calculate the Eigenvalues and Eigenvectors are determining from the correlation coefficient array.

(7)

Where λ_k is an eigenvalue, , and k = 1,2…n; $S_{ik} = [a_{k1}, a_{k2}…,a_{kn}]$ correspond to Eigen value λ_k.

4. The principal component is formulated as follows;

$P_{mk} =$ (8)

Where P_{m1} is the first principal component, P_{m2} is the second principal component and so on.

PCA is used to determine the corresponding weighting values for each quality characteristic. The trials of array for multiple quality characteristics listed in Table 4.8 represented the grey relational coefficient of each quality characteristic. These data used to assess the correlation coefficient matrix and determine the Eigen values from equation (7) is shown in Table 4.9. The Eigen vector corresponding to each Eigen value is listed in Table 4.10 and its square is represented the contribution of the corresponding quality characteristic to the principal component.

Table 4.9 Eigen values and explained for principal component

Principal component	Eigen value	Explained variation (%)
First	1.643	54.775
Second	0.97	32.34
Third	0.385	12.885

Table 4.10 Eigen vector for principal component

Quality characteristic	First	Second	Third
Penetration Depth	0.528	-0.672	-0.52
Width	0.483	0.741	-0.467
Distortion	0.699	-0.005	0.715

The contribution of responses in the penetration depth, weld width and distortion of the A-TIG weldment is shown in Table 4.11. These contributions were listed as 0.461, 0.203 and 0.336 respectively. Moreover the variance contribution for the first principal component characteristic the three quality characteristic was as high 54.775%. Therefore, for this study the squares of the

respective Eigen vectors were selected as the weighting values of the related quality characteristic. Coefficients c_1, c_2, and c_3 were set as 0.461, 0.203, and 0.336 respectively

Table 4.11 Contribution of each quality characteristic for the principal component

Quality characteristic	Contribution
Penetration Depth	0.461
Width	0.203
Distortion	0.336

Step 4- Grey Relational Grade

The average of the grey relational coefficient is then calculated to obtain grey relational grade. The grey relational grade is defined as follows:

$$\gamma_i = \qquad (9)$$

However the effect of each factor on the system is not exactly the same in real application. Thus equation (9) can be modified as follows:

$$\gamma_i = \qquad (10)$$

where c_k represents the normalized weighting value of factor k.

Using equation (10) and the data is listed in Table 4.8 and Table 4.11 the grey relational grades were evaluated as follows:

$$\gamma_1 = (0.461 \times 0.367) + (0.203 \times 0.527) + (0.336 \times 0.768) = 0.534$$

By using the same procedure , the grey relational grade of the comparability sequence for i = 1-18 can be obtained and is presented in Table 4.12. The processing parameters were optimized with respect to single grey relational grade rather than complicated multiple quality characteristics.

Table 4.12 Grey Relational Grade and its order

Trial	Grade	Order
1	0.53421698	9
2	0.586462123	7
3	0.437443104	16
4	0.403252073	17
5	0.445670177	15

6	0.497069623	11
7	0.839239464	1
8	0.675111141	5
9	0.522036259	10
10	0.689891878	4
11	0.460898957	13
12	0.459086826	14
13	0.49578924	12
14	0.55*2636072	8
15	0.371410411	18
16	0.698504546	3
17	0.596764092	6
18	0.776679271	2

In G-PCA, the grey relational grade is used to show the relationship between quality characteristics. If two sequences are same, the value of the grey relational grade is equal to one. The grey relational grade is also indicated the degree of manipulate that the comparability sequence can exert over the reference sequence.

Step 4 – Optimal combination of process parameters:

To determine the optimal combination of process parameters for responses in penetration depth, weld width and distortion of the A-TIG welding. The average grey relational grade for each process parameters level was evaluated by employing the main effect analysis of the Taguchi method. This process was performed by sorting the grey relational grades corresponding to the levels of the process parameters in each column of the OA and then taking the average of parameters with the same levels. i.e. for factor An experiments 1, 2, and 3 were set to level 1. Therefore by using the data listed in Table 4.12, the average grey relational grade for A_1 was evaluated as follows:

$A_1 =$ $= 0.544$
$A_2 =$ $= 0.468$
$A_3 =$ $= 0.675$

By using a similar method, evaluations were performed for each process parameter level and the main effect analysis was developed which is shown in Fig. 4.1 Considering that the grey relational grade was represented the level of correlation between the reference and comparability sequence. A larger grey relational grade was indicated that the comparability sequence exhibited stronger correlation with the reference sequence. Fig. 4.1 shown that the multiple quality

characteristics of the A-TIG welding were significantly affected by changing the processing parameters. From the response table for the grey relational grade shown in Table 4.13, the best combination of process parameters was A_3 (current of 140 A), V_1 (welding speed of 100 mm/min), and F_2 (mixture of flux TiO_2 and SiO_2).

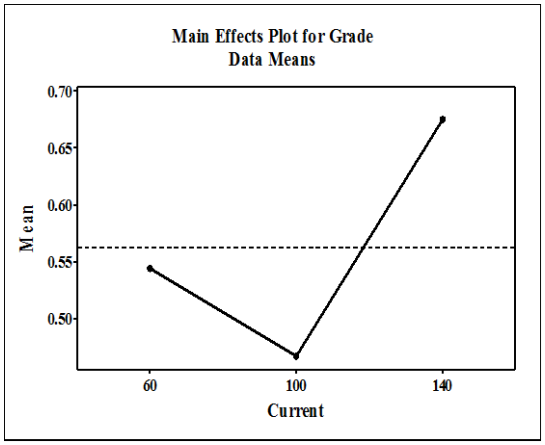

(a) Current

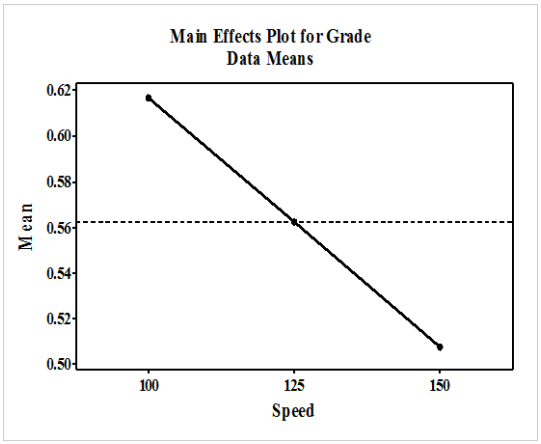

(b) Speed

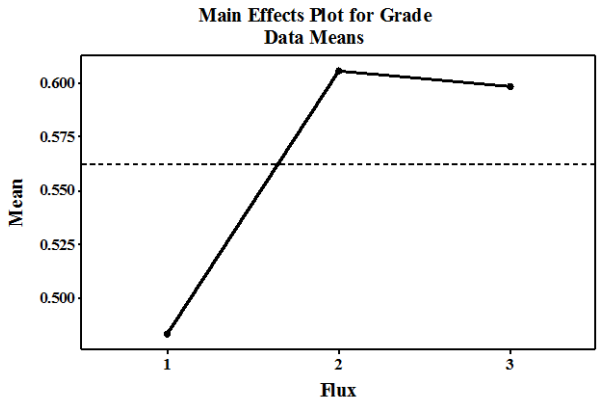

(c) Flux

Figure 4.1 Effect of process parameter levels on multiple quality characteristics

Table 4.13 Response table for grey relational grade

Symbol	Process parameter	level 1	Level 2	Level 3
A	Current	0.544	0.468	**0.675**
V	Speed	**0.617**	0.563	0.508
F	Flux	0.483	**0.606**	0.598

Step 5- Analysis of Variance (ANOVA)

ANOVA analysis is carried out using Minitab software. ANOVA was used to determine which parameter was significantly affected the quality characteristics. The results of ANOVA for the

grey relational grades are listed in Table 4.14. It shows that the two parameters current and flux are found to be the major factors with the selected multiple quality characteristics. The significance of each process parameter in the responses in penetration depth, weld width and distortion of the A-TIG welding process can be determined by the percentage contribution.

Table 4.14 Result of ANOVA

Symbol	Process Parameter	DOF	SS	MS	F-value	Contribution (%)
A	Current	2	0.1311	0.0656	14.23	47.81
V	Speed	2	0.0359	0.0179	3.89	13.09
F	Flux	2	0.0565	0.0283	6.13	20.61
Error		11	0.0507	0.0046		18.49
Total		17	0.2742			

From the results of ANOVA, current appearances to be most important processing parameter with the highest percentage contribution of 47.81% which increases penetration depth and reduces weld width as well as distortion of the A-TIG welding.

4.5 Summary

The A-TIG welding process parameters are optimized for penetration depth, weld width and angular distortion using G-PCA. The input parameters like welding current, welding speed and activated flux have great influence in deciding the weld quality. The ANOVA of G-PCA for multiple performance characteristics revealed that welding current and activated flux are the most influential parameters. The optimum levels of process parameters are welding current 140A, welding speed 100 mm/min and SiO_2+TiO_2 mixture of activated flux.

Chapter 5: Parametric effect on A-TIG welds

5.1 Introduction

After got optimum parameters by optimization technique, the effect of parameters on macrostructure, microstructure and angular distortion of stainless steel 304L in A-TIG welds have been explained in this chapter.

5.2 Effects of A-TIG welding on Surface Appearance

Fig. 5.1 shows the surface appearance of 304L stainless steel TIG welds with and without flux under welding conditions. Fig. 5.1a shows the results of TIG welding without flux which was produced smooth and clean surface. Fig 5.1b shows that the use of TiO_2+MnO_2 flux was produced excessive residual slag and small spatters. Fig. 5.1c shows a satisfactory surface appearance for the 304L stainless steel weld was obtained while using SiO_2+TiO_2 flux. Fig. 5.1d shows that using Al_2O_3+CaO flux was produced little residual slag and large spatters. These results were clearly indicated that on 304L stainless steel, SiO_2+TiO_2 powder was produced TIG welds with a satisfactory surface appearance but while using other two combination fluxes were produced to the formation of slag and spatters. It was happened because oxide compounds have substantially higher melting point, boiling point and thermal decomposition temperature than fluoride and sulfide compounds. Oxide powders were not easily melted by the arc heat source of TIG welding. It was indicated that TIG weld was produced with oxide fluxes contributed to the formation of residual slag.

(a) Without Flux

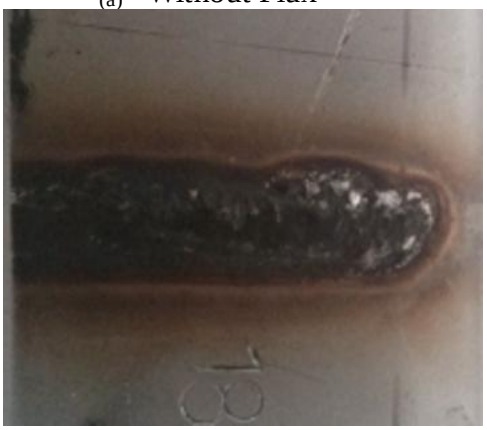

(b) With TiO_2 + MnO_2

(c) With SiO_2+TiO_2

(d) With Al_2O_3+CaO

Figure 5.1 Effect of oxide flux on surface appearance

5.3 Effects of A-TIG welding on weld morphology

Fig. 5.2 is presented the cross section of stainless steel TIG welds produced without and with oxide flux powders. Fig 5.2a and d show the results of TIG welding without flux and with TiO_2+MnO_2 powder which was produced shallow, wide penetration. Fig 5.2b and Fig. 5.2c show that SiO_2+TiO_2 and Al_2O_3+CaO powders were produced deep and narrow penetration. In the experiments, SiO_2+TiO_2 powder was facilitated complete penetration in 304L stainless steel TIG welds. Al_2O_3+CaO and TiO_2+MnO_2 can capable of increasing penetration depth of TIG welds. A weld with high penetration depth was indicated that energy density of the heat source was increased in welding which was produced high concentration of heat energy during welding. The energy density of heat source was increased the overall heat required per unit length of the weld was decreased. It was indicated that A-TIG welding was also achieved higher melting efficiency. A-TIG welding was significant reduce the amount of heat required for the welds with large cross section area and high weld depth.

Current-140A Speed-125 mm/min
Penetration- 1.16mm Width- 5.65mm
(a) Without flux

Current-140A Speed-125 mm/min
Penetration- 3.38mm Width- 3.95mm
(b) With SiO_2 + TiO_2

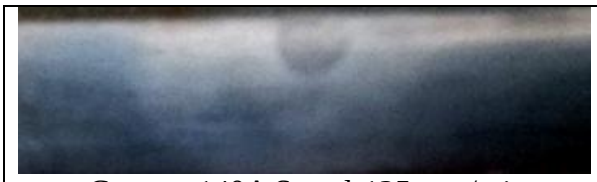

Current-140A Speed-125 mm/min
Penetration- 2.34mm Width- 2.51mm
(c) With Al_2O_3 + CaO

Current-140A Speed-125 mm/min
Penetration- 1.29mm Width- 5.99mm
(d) With TiO_2 + MnO_2

Figure 5.2 effect of TIG welds with various flux powders on weld morphology

5.4 Effects of A-TIG welding on angular distortion

Deformation was occurred due to solidification shrinkage and thermal contraction in weld pool and base metal during quickly heating and cooling cycle. Fig. 5.3 show the angular distortion of TIG welding was made with and without different combination of oxide compound. A-TIG welding was increased penetration joint and decreased angular distortion. It was characteristic of high degree of energy concentration during welding and reduced the quality of supplied heat. It was prevented to overheat of the base metal and reduced the incidence of thermal strains and incompatible strain was caused by shrinkage in thickness [15]. As a result, angular distortion was reduced of 304L stainless steel A-TIG weldments. The angular distortion of the weldment made with mixture of SiO_2 and TiO_2 was reduced compared with other two combinations. The angular distortion of weldment was depended on the ratio of the weld depth and plate thickness and it was also depended on power density of the welding heat source. It was increased with increasing weld current.

Figure 5.3 Angular distortions of A-TIG weldments

Angular distortion of weldment was decreased at shallow depth and increased with increasing ratio of penetration depth and plate thickness in A-TIG welding process to critical point at 100 A. When penetration depth was exceed half of plate thickness the angular distortion was decreased at current greater than 100 A. Penetration depth was increased and angular distortion was decreased in A-TIG welding which was indicated that arc was generated with higher energy density. As the arc energy density was increased the overall heat energy required per unit length of weld deposit was decreased. Consequently, A-TIG welding was capable of reducing the angular distortion of weldment.

5.5 Effects of A-TIG welding on microstructure

Microstructure examination of any material is depended on its chemical composition and various process parameters used by the welding. The experiments used type 304L stainless steel plates as a base metal. The microstructure examination was carried out using Inverted Optical Microscope with image analyzer. The cross section of samples were fine polished and etched by etching solution of 10g $CuSO_4$ with 100 ml HCl to examine the microstructure of FZ, HAZ and fusion boundary. Fig 5.4 shows the microstructure of 304L stainless steel base metal consists of tempered martensite and the grain size is smaller compared to that of the grain size in the fusion zone of weld joint. Fig 5.5 shows the microstructure of 304L stainless steel weld metal at fusion zone and HAZ were produced with and without flux. Grain size was measured by line intersecting method at fusion zone of TIG and A-TIG weldments. Fig. 5.5(a) shows that the average value of grain size is 18.4µm while using TIG welding without flux. Fig. 5.5(b) shows that the average value of grain size is 30.95µm while using Al_2O_3 + CaO flux. Fig. 5.5(c) shows that the average value of grain size is 26.85µm while using TiO_2 + MnO_2 flux. Fig. 5.5(d) shows that the average value of grain size is 21.9µm while using TiO_2 + SiO_2 flux. Results are indicated that the denderitic arm spacing and the HAZ grain size are increased while using activated flux in TIG welding. It was also seen that the delta ferrite was increased than the base metal. This is because most of the weld metal of stainless steel was solidified as delta ferrite phase. During welding, the cooling rate of the weld metal was so quickly that the phase transformation of delta ferrite to austenite was not complete. Delta ferrite was retained more in the weld metal after solidification.

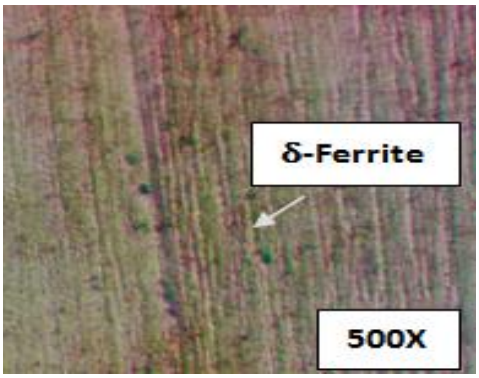

Figure 5.4 Microstructure of 304L stainless steel base metal

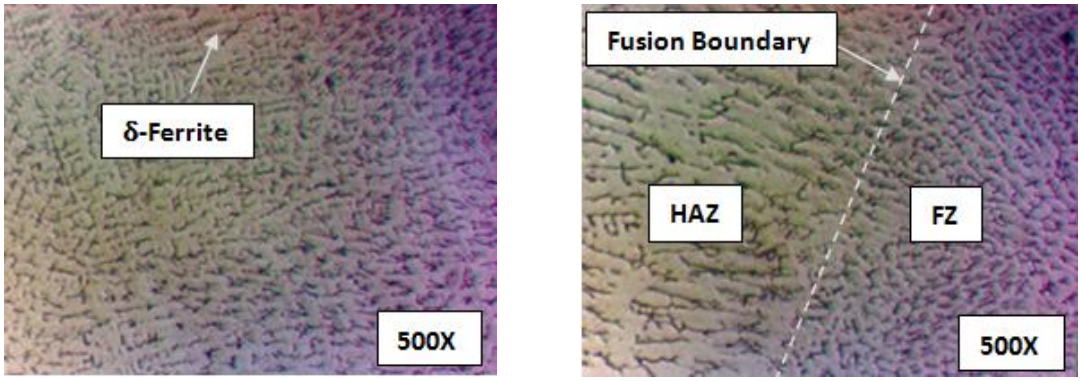

(a) Without flux

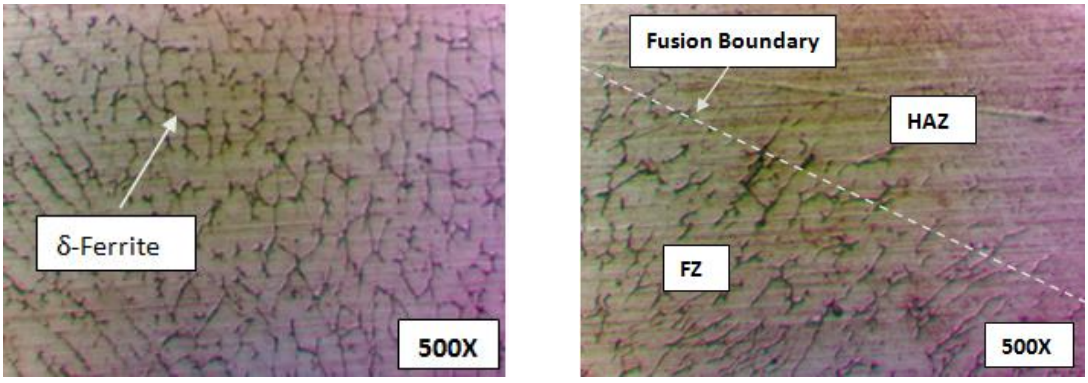

(b) With Al_2O_3 + CaO Flux

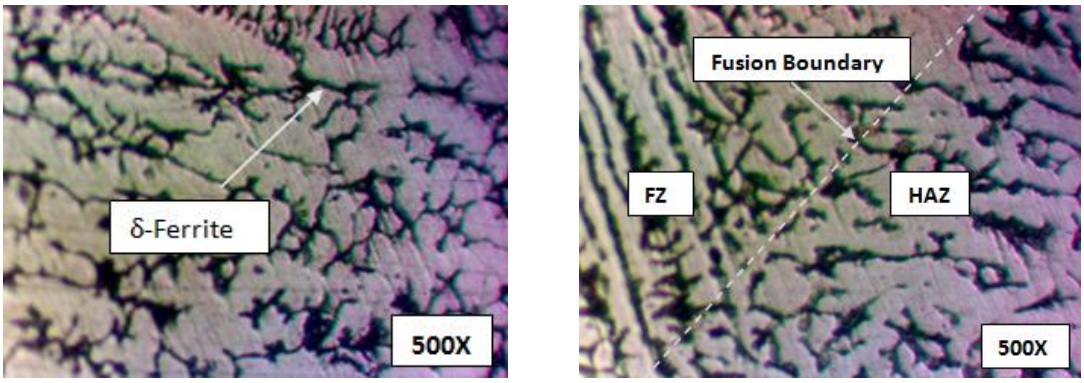

(c) With TiO_2 + MnO_2 Flux

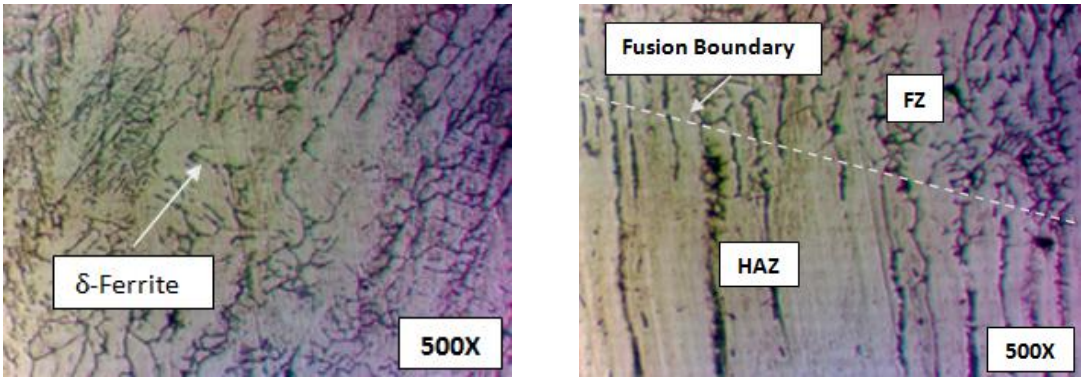

(d) With TiO_2 + SiO_2 Flux

Figure 5.5 effect of activated flux on microstructure

When using oxide flux, the delta ferrite content was increased than TIG welding process. This result was related to the heat input during TIG welding with oxide flux. When TIG welding was used with oxide flux the arc voltage was increased. This effect was increased the anode current density and the arc force was acting on the weld metal. The experiment results show that while using activated flux the arc voltage was slightly increased due to "Arc Constriction" [15]. The heat input was proportional to the arc voltage and activated flux has been positive effect of increasing the heat input unit length of weldments. The higher heat input could increase the peak temperature of the weld and more delta ferrite forms in the A-TIG weldments. It was ascribed to the thermal cycling and recrystallization occurred due to the activated flux. All cases were exhibited microstructure of austenite matrix and vermicular delta ferrite morphology typical of the type of material.

6. Conclusion

This is presented that optimization of process parameters of A-TIG welding by using Grey Relational Analysis (GRA) coupled with Principal Component Analysis (PCA) and to investigate the influence of different kinds of oxide fluxes on the welds. The conclusion can be drawn below:

1) TIG welding with mixture of SiO_2 and TiO_2 fluxes achieves increase in weld depth and decrease in weld width as well as angular distortion.

2) The results indicate that TIG welds produced without flux the surface appearances clean and smooth but with flux formed residual slag, spatters and small amount of fume is reported.
3) The G-PCA method is supplemented by the ANOVA which is revealed that current, speed and flux are controllable factors significantly the multiple quality characteristics with desire contribution of 47.81%, 13.09% and 20.61% respectively.
4) The optimal combination of the process parameters was obtained from the proposed method was set with values of current, speed and flux 140 A, 100 mm/min and mixture of SiO_2 and TiO_2 flux respectively. The corresponding responses are penetration depth, weld width and distortion of 3.64mm, 3.76mm, and 0.76 respectively.
5) The A-TIG welding can increase the arc voltage, the amount of heat input per unit length in weld is also increased and therefore the delta ferrite content in weldments is increased. It is also noticed that the grain size is increased at HAZ while using activated flux in TIG welding.

References

1. Cheng-Hsien Kuo, Kuang-Hung Tseng and Chang-Pin Chou, Effect of activated TIG flux on performance of dissimilar welds between mild steel and stainless steel, Key Engineering Materials 479 (2011) 74-80
2. LI Qing-ming, WANG Xin-hong, ZOU Zeng-da, WU Jun, effect of activated flux on arc shape and arc voltage in TIG welding, Trans. Nonferrous Met. Soc. China I7(2007) 486-490
3. Kuang-Hung Tseng, Development and application of oxide- based flux powder for tungsten inert gas welding of austenitic stainless steel, Powder Technology 233 (2013) 72–79
4. Yoshiaki Morisada, Hidetoshi Fujii, Ni Xukun, Development of simplified active flux tungsten inert gas welding for deep penetration, Materials and Design 54 (2014) 526–530
5. Magudeeswarang G, Sreehari R. Nair, L. Sundar, N. Harikannan, Optimization of process parameters of the activated tungsten inert gas welding for aspect ratio of UNS S32205 duplex SS welds, Define technology (2014)1-10
6. A. Berthier, P. Paillard, M. Carin, F. Valensi and S. Pellerin, TIG and A-TIG welding experimental investigations and comparison to simulation Part 1: Identification of Marangoni effect, Science and technology of welding and joining 17 (8) (2012) 609-615
7. T. Sakthivel , M. Vasudevan, K. Laha, P. Parameswaran, K.S. Chandravathi, M.D. Mathew, A.K. Bhaduri, Creep rupture strength of activated-TIG welded 316L(N) stainless steel, Journal of nuclear materials 413 (2011) 36-40
8. E. Ahmadi, A. R. Ebrahimi, R. Azari Khosroshahi, Welding of 304L Stainless Steel with Activated Tungsten Inert Gas process (A-TIG), International journal 10 (1) (2013) 27-33
9. Paulo J. Modenesi, Eustaquio R. Apolinario, Iaci M. Pereira, TIG welding with single component fluxes, Journal of Materials Processing Technology 99 (2000) 260-265

10. Shanping Lu, Hidetoshi Fujii, Hiroyuki Sugiyama, Manabu Tanaka, Kiyoshi Nogi, Weld Penetration and Marangoni convection with Oxide Fluxes in GTA Welding, Material Transactions 43 (11) (2002) 2926-2931
11. Y.L.Xu, Z.B Dong, Y.H. Wei, C.L.Yang, Marangoni convection and weld shape variation in A-TIG welding process, Theoretical and Applied Fracture Mechanics 48 (2007) 178–186
12. B. Arivazhagan, M. Vasudevan, A comparative study on the effect of GTAW processes on the microstructure and mechanical properties of P91 steel weld joints, Journal of Manufacturing Processes 16 (2014) 305–311
13. Kuang-Hung Tseng, Ko-Jui Chuang, Application of iron based powders in tungsten inert gas welding for 17Cr-10Ni-2Mo alloys, Powder Technology 228 (2012) 36–46
14. P. Vasantharaja, M. Vasudevan, Studies on A-TIG welding of Low Activation Ferritic/Martensitic (LAFM) steel, Journal of Nuclear Materials 421 (2012) 117–123
15. Kuang-Hung Tseng, Chih-Yu Hsu, Performance of activated TIG process in austenitic stainless steel welds, Journal of Materials Processing Technology 211 (2011) 503–512
16. Tsann-Shyi Chern, Kuang-Hung Tseng, Hsien-Lung Tsai, Study of the characteristics of duplex stainless steel activated tungsten inert gas welds, Materials and Design 32 (2011) 255–263
17. G. Ruckert, B. Huneau, S. Marya, Optimizing the design of silica coating for productivity gains during the TIG welding of 304L stainless steel, Material and Design 28 (2007) 2387-2393
18. Kuang-Hung Tseng, Nai-Shien Wang, GTA welding assisted by mixed ionic compounds of stainless steel, Powder Technology 251 (2014) 52–60
19. Sanjay G. Nayee, Vishvesh J. Badheka, Effect of oxide based fluxes on mechanical and metallurgical properties of Dissimilar Activating Flux Assisted-Tungsten Inert Gas Welds, Journal of Manufacturing Processes 16 (2014) 137–143